Structure and Function of 6,7-Dicarboxyheme-Substituted Myoglobin†

Saburo Neya,*,‡ Noriaki Funasaki,‡ Noriyuki Igarashi,§ Akira Ikezaki,§ Takao Sato,|| Kiyohiro Imai,⊥ and Nobuo Tanaka*,§

Department of Physical Chemistry, Kyoto Pharmaceutical University, Yamashina, Kyoto 607, Japan, Faculty of Bioscience and Biotechnology, Department of Life Sciences, Tokyo Institute of Technology, Midori-ku, Yokohama 226, Japan, Department of Biological Science and Technology, Faculty of Engineering, The University of Tokushima, Tokushima 770, Japan, and Department of Physicochemical Physiology, Medical School, Osaka University, Suita, Osaka 565, Japan

Received October 23, 1997; Revised Manuscript Received January 22, 1998

ABSTRACT: Myoglobin was reconstituted with 6,7-dicarboxy-1,2,3,4,5,8-hexamethylheme, a compact synthetic heme with the shortest acid side chains, to pursue the structural and functional consequences after intensive disruption of the heme propionate−apoglobin linkages in the native protein. The electron-withdrawing carboxylate groups directly attached to the porphyrin ring lowered the oxygen affinity by 3-fold as compared with native myoglobin. Autoxidation of the oxy derivative to the ferric protein proceeded with 1.6×10^{-2} min^{-1} at pH 7.0 and 30 °C. The crystallographic structure of the cyanomet myoglobin with 1.9 Å resolution shows that the heme adopts a unique orientation in the protein pocket to extend the two carboxylates toward solvent sphere. The native globin fold is conserved, and the conformations of globin side chains are almost intact except for those located nearby the heme 6,7-carboxylates. The 7-carboxylate only weakly interacts with Ser92 and His97 through two mediating water molecules. The 6-carboxylate, on the other hand, forms a novel salt bridge with Arg45 owing to conformational flexibility of the guanidinium side chain. The proton NMR shows that the small heme does not fluctuate about the iron−histidine bond even at 55 °C, suggesting that the salt bridge between Arg45 and heme 6-carboxylate is of critical importance to recognize and fix the heme in myoglobin.

Iron porphyrin serves as the prosthetic group of hemoprotein. The peripheral substituents are suggested to stabilize holoprotein through a number of specific heme−apoprotein contacts. The hemes with modified substituents are unique tools to perturb the heme−globin interactions. Intensive chemical modification has been carried out for the 2,4-vinyl groups of protoheme (*1*), and the functional role of the heme vinyl groups has been assessed (*2*−*4*). The propionate groups are uniformly found in various types of naturally occurring hemes (*5*). The propionates are suggested to be one of the major factors to accommodate the heme in a unique orientation in proteins via hydrogen-bonding networks (*6*−*9*). Coletta et al. (*10*) further proposed that the cooperative interactions in clam hemoglobin are transmitted to a large extent through the heme propionates.

Roles of heme propionates in protein have been evaluated for recent years by genetically engineered proteins (*6*−*9, 11*) or by introduction of polypropionates to the heme ring (*12*−*14*). Another fundamental and promising approach is the chemical modification of propionate groups themselves. We prepared 6,7-dicarboxy-1,2,3,4,5,8-hexamethylheme, a new type of heme with the shortest acid side chains (inset, Figure 1). The heme is formally derived from protoheme by replacing the 2,4-vinyls with small methyls and shortening each of the 6,7-propionates by two methylene carbons. The resultant compact molecular structure refers to enhanced mobility of the heme in myoglobin, Mb[1] (*15*−*18*). In addition, shortening of heme propionate inevitably modifies the hydrogen bonding frameworks formed in native Mb (*19, 20*). It is also expected that the strongly electron-withdrawing carboxylates at heme periphery affect reactivity of the central iron. We addressed the following questions to the novel prosthetic group. How does the globin recognize the dicarboxy heme? What structural rearrangements will be caused around the direct vicinity of heme carboxylates? What are the functional consequences? We carried out detailed structural and functional characterizations of the reconstituted Mb to evaluate the roles played by the heme carboxylates.

MATERIALS AND METHODS

6,7-(Diethoxycarbonyl)-1,2,3,4,5,8-hexamethylporphyrin and Hemin. A 100 mL of ethanol containing 1 mL of sulfuric acid, 4,4′-dimethyl-3,3′-(diethoxycarbonyl)dipyrromethane-5,5′-dialdehyde (200 mg, 0.53 mmol) (*21*), and 3,3′,4,4′-tetramethyldipyrromethane-5,5′-dicarboxyic acid (155 mg, 0.53 mmol) (*22*) was refluxed for 5 h. The cooled

† This work was supported by the grant-in-aid from the Scientific Research Foundation of Kyoto Pharmaceutical University.

* To whom correspondence should be addressed. *e*-mail, sneya@mb.kyoto-phu.ac.jp.

‡ Kyoto Pharmaceutical University.

§ Tokyo Institute of Technology.

|| The University of Tokushima.

⊥ Osaka University.

[1] Abbreviations: Mb, myoglobin; NMR, nuclear magnetic resonance: Tris, tris(hydroxymethyl)animomethane; ppm, parts per million.

S0006-2960(97)02632-9 CCC: $15.00
Published on Web 03/31/1998

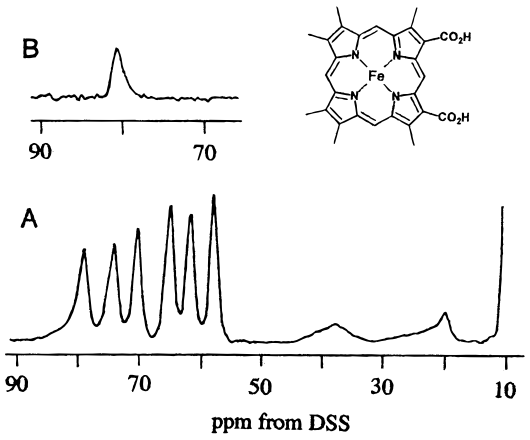

FIGURE 1: Proton NMR spectra of the Mb reconstituted with 6,7-dicarboxy-1,2,3,4,5,8-hexamethylheme in 0.1 M Tris at 20 °C: (A) Aquomet Mb in D_2O, pD 7.0; (B) exchangeable proton region of deoxy Mb in H_2O, pH 7.0. Inset denotes the structure of the prosthetic group. DSS = sodium 2,2-dimethyl-2-silapentane-5-sulfonate.

mixture was poured into 500 mL water and extracted with chloroform (100 mL × 3). The chloroform solution was washed with aqueous sodium bicarbonate, dried with magnesium sulfate, and evaporated to dryness. The residue was chromatographed on a silica gel column (Wako C-200, Wako Pure Chemicals, Osaka, Japan) with chloroform/methanol (100/4, v/v). The purified porphyrin diethyl ester (77.0 mg, 27%) was crystallized from chloroform/methanol as fine black needles. Anal. Calcd for $C_{32}H_{34}N_4O_4$: C, 71.35; H, 6.36; N, 10.40. Found: C 71.61; H, 6.17; N, 10.72. Mass: *m/e* 538, calcd for M^+ *m/e* 538.7. δ_H (chloroform-*d*): −3.81 (2H, br s, NH), 1.83 (6H, t, CH_2CH_3), 3.50 (12H, s, ring CH_3), 3.91 (6H, s, ring CH_3), 4.92 (4H, q, CH_2CH_3), 9.75 (H, s, meso H), 9.94 (2H, s, meso H), 11.83 (H, s, meso H). λ_{max} (and ϵ) (chloroform): 417 nm (188 mM^{-1} cm^{-1}), 511 (12.0), 548 (9.5), 582 (6.1), and 637 (4.2).

The pK_3 of the pyrrole NH was spectrophotometrically determined at 20 °C after Hambright (*23*). The porphyrin diethyl ester dissolved in sulfuric acid was diluted with unbuffered water containing 2.5% sodium dodecyl sulfate to a concentration with an optical absorbance of 1.6 at 415 nm. The solution was carefully adjusted to pH 5 with 0.1 M NaOH. The solution was acidified to pH 2 after successive addition of dilute hydrochloric acid. The absorption changes were analyzed with a Henderson−Hasselbalch equation.

The ferric porphyrin chloride, prepared with the porphyrin and ferrous chloride in refluxing dimethylformamide (*24*), was purified with silica gel column chromatography (chloroform/methanol, 100/3 by volume). After the ester side chains were hydrolyzed (*25*), the hemin was precipitated with hydrochloric acid and dried.

Reconstituted Mb. Sperm whale Mb was purchased from Sigma (type II). The apoprotein (*26*) was mixed with a 1.2-fold molar excess of the hydrolyzed hemin dissolved in a small volume of 50 mM sodium hydroxide. The crude mixture was dialyzed overnight against cold 10 mM Tris at pH 7.0. The solution was loaded on a carboxymethylated cellulose (Whatman, CM-52) column equilibrated with the same buffer and eluted with 0.1 M Tris, pH 7.0. A typical reconstitution yield was 80%. The aquomet Mb was determined with $\epsilon_{408} = 148$ mM^{-1} cm^{-1} that is based on the pyridine hemochromogen spectrum, $\epsilon_{519} = 22.6$ or $\epsilon_{552} = 27.2$ mM^{-1} cm^{-1}, recorded as described by Antonini and Brunori (*27*).

Mb Crystallization and X-ray Structural Determination. The reconstituted Mb was crystallized by a batch method with ammonium sulfate as the precipitant. Powdered ammonium sulfate was added to 300 μL of 11 mg/mL protein solution containing 50 mM Tris-HCl buffer, pH 7.0, and 10 mM potassium cyanide until slight turbidity was persistently observed. The final concentration of ammonium sulfate was 3.7 M. One month later at 4 °C crystals with a size of 0.7 × 0.7 × 0.2 mm^3 appeared. The space group *P*6 and the unit cell dimension $a = b = 91.02$ and $c = 45.68$ Å were determined according to Sato et al. (*28*).

Two sets of diffraction data were measured on a Rigaku R-AXIS IIc with two crystals mounted so that the b^* and c^* axes were parallel to the spindle axes, respectively. The data were collected at a detector distance of 90 mm with 60 oscillation frames after 30-min exposure. The oscillation range was 1.2°/frame to integrate the reflections. These frames were processed and scaled after Higashi (*29*). The resultant two independent sets of data were merged into a single-intensity set with 95% completeness.

The structure was refined with the XPLOR program (*30*). Native metMb structure (*19*) was employed as a starting model. Solvent molecule and heme were initially excluded. After 50 cycles of preliminary rigid-body refinement, the electron density of heme became clear in the difference Fourier map. The heme model was built prior to subsequent refinement. The initial *R*-factor converged to 0.283 for the data between 10 and 2.5 Å resolution. A typical refinement included the simulated annealing, energy minimization, and individual *B*-factor refinement for all atoms. The $(F_o - F_c)$ and $(2F_o - F_c)$ difference maps calculated in XPLOR were visualized with the graphics program FRODO (*31*) to permit manual rebuilding of misplaced side chains. The peaks larger than four standard deviations in the $(F_o - F_c)$ maps were modeled as water molecules if they are located at reasonable distances from the protein and other solvent molecules. The atomic coordinates of the CN ligand were included for phasing only in the final refinement cycle to avoid biasing the diatomic ligand position. When the iron ligand and sulfate ion are resolved in the maps, manual fitting was performed on the graphics. The manual refinement was repeated until no further convergence of the *R*-factor was achieved. The statistics of data and refinement are summarized in Table 1. The coordinates and temperature factors of the final atomic model have been deposited in the Protein Data Bank, Brookhaven National Laboratories, under an accession number 1IOP.

Spectroscopic Observation and Ligand Binding Measurements. The electronic absorption spectra were recorded on a Shimadzu MPS-2000 spectrophotometer with a thermostated cell compartment. Ligand binding and acid−alkaline transition were monitored with the spectrophotometer. Proton NMR spectra at 300 MHz were obtained with a Varian XL-300 spectrometer with 1−3 mM Mb solutions. Equilibrium oxygen binding was examined with the automatic recording apparatus (*32*) in the presence of a reducing system (*33*) in 0.1 M phosphate at pH 7.3 and 25 °C. The equilibrium process was examined over a partial oxygen-

Table 1: Statistics of Data Collection and Refinement of the Reconstituted Mb

no. of cryst	2
space group	*P*6
cell params (Å)	$a = b = 91.02$, $c = 45.68$
tot. reflcns	185 449
indepdt reflcns	17 073
reflcns used in refinement	16 116
R_{merge}[a]	0.067
R_{cryst}[b]	0.195
data completeness: all shells; final shell (1.99−1.90)	0.963; 0.944
resolution range of refinement (Å)	10.0−1.9
no. of atoms	
pepetide	1217
heme group	39
water molecule	136
sulfate ion	1
root-mean-squares	
in bond lengths (Å)	0.007
in bond angles (deg)	1.645
av temp factors (Å^2)	
overall struct	24.25
main chain	20.29
side chain	24.15
prosthetic group	15.33
solvent	44.35

[a] R_{merge} is the unweighted *R*-factor on the reflection intensities among symmetry mates. [b] $R_{cryst} = \Sigma(|F_o| - |F_c|)/\Sigma(|F_o|)$

Table 2: Visible Absorption of the Mb-Containing 6,7-Dicarboxy-1,2,3,4,5,8-hexamethylheme

Mb[a]	λ (nm) (ϵ, mM^{-1}cm^{-1})			
		Ferric		
H_2O	397 (163)	500 (6.4)	574 (2.7)	627 (3.1)
CN^-	416 (124)	540 (8.9)		
		Ferrous		
deoxy	427 (122)	550 (10.0)		
O_2	406 (91)	537 (9.2)	573 (6.7)	
CO	415 (173)	536 (11.7)	562 (8.5)	

[a] In 0.1 M Tris at pH 7.0 and 20 °C.

pressure range of 1−150 mmHg. Autoxidation of the oxy complex was spectrophotometrically monitored at the Soret peak in 0.1 M Tris buffer, pH 7.0, and 30 °C.

RESULTS

Electronic Influences of Heme Carboxylates. The electron-withdrawing carboxy groups affect acidity of the pyrrole nitrogens. The influence is quantitatively estimated from the pK_3 of porphyrin (*23*). Analysis of the pH-dependent absorption decrease at 415 nm afforded a p$K_3 = 2.9 \pm 0.2$ for the free-base porphyrin. The observed value, lower than 4.8 of protoporphyrin (*23*), is close to p$K_3 = 3.0$ of diformylporphyrin (*34*). Consistent with the small pK_3 value, the 600-nm absorption maximum that is a qualitative marker of porphyrin acidity (*5*) occurs at 637 nm. Thus, the dicarboxy porphyrin is more acidic than protoporphyrin.

Reconstituted Mb. Optical titration of the apoMb with the hemin revealed a clear inflection point at a 1:1 binding stoichiometry. Purified metMb exhibited an absorbance ratio $A_{408}/A_{280} = 5.2$. The visible spectrum (Table 2) with dominant 500 and 630 nm bands suggests its aquomet form and is remarkably pH-dependent. The acid−alkaline transition occurred at pH 8.8 ± 0.1. Figure 1 shows the NMR spectrum of the aquomet Mb, where the six heme methyls are observed at 57.7, 61.6, 64.9, 70.2, 74.0, and 78.7 ppm. A single set of the heme methyl peaks demonstrates that the heme adopts a unique orientation in Mb owing to the molecular symmetry about the α,γ-*meso*-carbon axis. The broad 38-ppm signal with four-proton intensity, assigned to the *meso*-protons of the hemin, indicates a 6-coordinate structure of Mb (*35*), consistent with the visible spectrum to show the presence of an iron-bound water molecule. The NMR of deoxy Mb confirms formation of the iron−histidine bond. The NH signal from the proximal imidazole was observed at 81.0 ppm to reflect the spin transfer from the heme to His93 through the iron−histidine bond (Figure 1).

Ligand Binding and Autoxidation. Cyanide binds to the ferric Mb (Table 2). The visible spectral analysis afforded an affinity of 1.2×10^6 M^{-1} in 0.1 M Tris at pH 7.0 and 20 °C. The reduced Mb is functionally active. The Hill plot of oxygen binding at pH 7.3 and 25 °C is characterized with a slope of 1.04 and an oxygen pressure at a half-saturation of 1.5 mmHg. The oxygen affinity, 3-fold lower than 0.5 mmHg of native Mb (*36*), is comparable with 2.8 mmHg reported for diformylheme-bound Mb (*34*). The visible spectra of the oxy, deoxy, and carbonmonoxy derivatives are summarized in Table 2. The peaks of each complex exhibit bathochromic shift by 3−6 nm relative to those found in the Mb with 2,4-dimethyldeuterioheme, a reference compound bearing heme propionates (*2*). The oxy Mb is not stable enough and apt to be autooxidized into aquomet Mb. The autoxidation proceeded with 1.6×10^{-2} min^{-1} at pH 7.0 and 30 °C. The rate is 13-fold larger than 1.2×10^{-3} min^{-1} of 2,4-dimethyldeuteroheme-substituted Mb (*2*). The accelerated autoxidation suggests easier access of solvent molecules to the heme distal site (*11, 37*).

Description of Crystallographic Model. We determined the structure of the cyanomet Mb at 1.9 Å to inspect details of the heme−globin interactions. The Mb crystallized in a *P*6 form in contrast with native Mb with a $P2_1$ crystal structure (*19, 20*). Crystal packing force has minimal influence on the tertiary structure of globin. We note a similar situation for native Mbs with two different crystal structures (*39*).

We compared the tertiary structure of the cyanomet Mb with that of isoelectronic native Mb complexed with CO (*20*). The globin fold is essentially intact after dicarboxyheme insertion (Figure 3). Standard deviation for the Cα positions along the backbone is only 0.47 Å while the overall error in the atomic coordinates, as estimated from a Luzzati plot (*38*), is between 0.20 and 0.25 Å. The significant deviations are observed in the solvent accessible parts and the C-terminal region contacting with another protein molecule in the crystal lattice.

Dicarboxyhemin is embedded in the protein pocket in an orientation almost identical with that of the protoheme (*19, 20*). The hydrophobic moiety of the porphyrin ring lies inside, and the hydrophilic 6,7-substituents point toward the globin surface (Figure 4). The proximal histidine coordinates to the heme iron. The direct vicinity of the small 2,4-methyls of porphyrin ring is less crowded. Accordingly, the dicarboxyhemin is inserted deeper by 0.5 Å than the protoheme (*19*). There are 85 protein contacts within 4 Å of the heme, close to 96 found for the protoheme in native Mb (*19*). The heme−globin contacts are profiled in Figure 4.

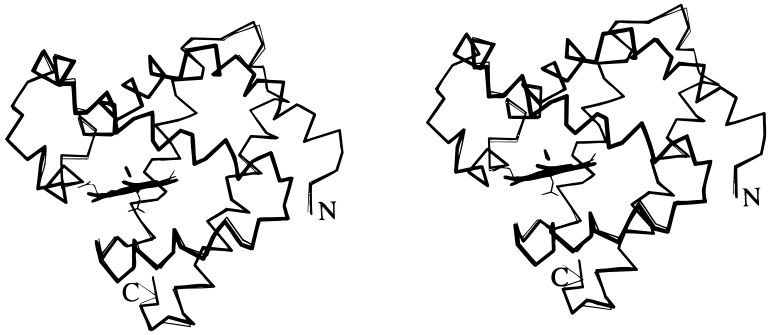

FIGURE 2: Stereodrawing of the Cα-backbones of the reconstituted cyanomet Mb (heavy lines) and native carbonmonoxy Mb (thin lines, *20*).

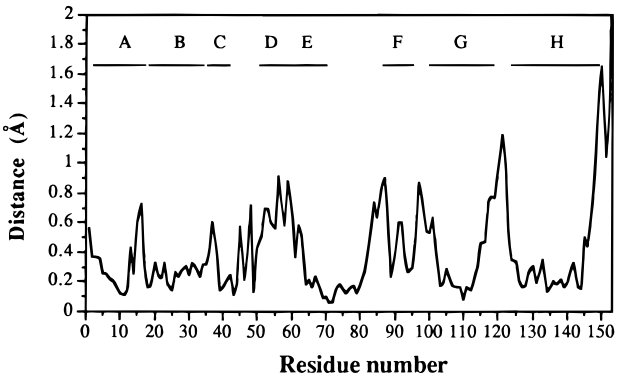

FIGURE 3: Deviations of Cα-positions after superposition of the two crystal structures of the reconstituted cyanomet Mb and native carbonmonoxy Mb (*20*).

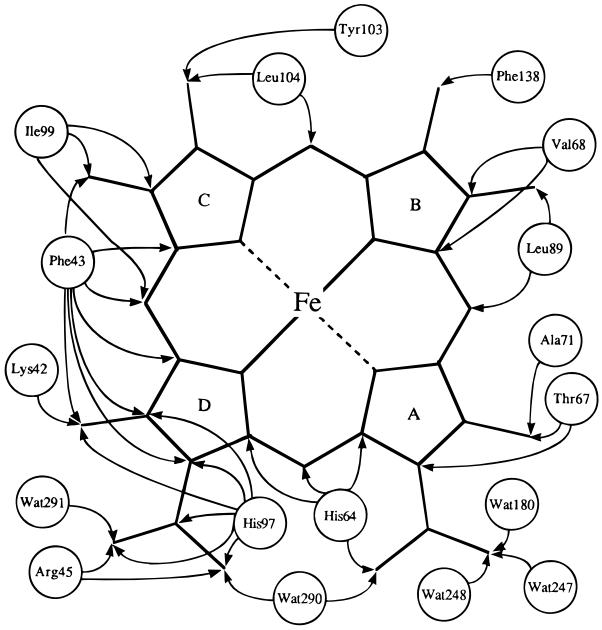

FIGURE 4: Heme−globin contacts within 4 Å of the 6,7-dicarboxy-1,2,3,4,5,8-hexamethylheme in sperm whale cyanomet Mb. The 6- and 7-carboxylates are those attached to the pyrrole rings D and A, respectively. This figure is to be compared with the corresponding drawing (*8*) for native Mb.

Changes in the Heme Carboxylate Region. The heme propionates in native Mb are hydrogen-bonded with the side chains of Arg45, Ser92, and His97 (*19, 20*). Deletion of two methylene carbons from each of the propionates should result in serious conformational shift of the hydrogen-bonding residues. The present X-ray structure reveals several intriguing results especially on the globin−carboxylate interactions. Details of the structural rearrangements around the heme carboxylates are illustrated in Figure 5. The conformations of the side chains in Ser92 and His97 are unexpectedly conserved. The largest movement was observed for Arg45 originally located at the protein surface. The guanidinium group of Arg45 remarkably swings into the inside by as much as 2.5 Å to form a novel salt bridge with the heme 6-carboxylate. The heme 6-carboxylate is also hydrogen-bonded with one water molecule, W291. On the other hand, the 7-carboxylate is too short to maintain the direct hydrogen bonds with Ser92 and His97. The 7-carboxylate in turn forms new hydrogen bonds with three water molecules, W180, W247, and W290. The two water molecules, W247 and W248, are accidentally settled at the same sites of the two terminal oxygen atoms of the heme 7-propionate in native Mb (*19, 20*) to form hydrogen bonds with Ser92 and His97. Accordingly, the 7-carboxylate, although indirectly, still gets in touch with Ser92 and His97 through the two intervening water molecules. These rearranged hydrogen bonds account for the unexpected preservation of the original configurations for the side chains of Ser92 and His97. It is also notable that the 6-carboxylate lies in almost parallel with the porphyrin ring whereas the 7-carboxy groups are twisted. The eclipsed conformation of the 6-carboxylate suggests possible resonance conjugation with the porphyrin macrocycle.

Coordination Structure. The coordination environment of the heme is illustrated in Figure 5. The proximal histidine binds to the iron with a bond distance of 2.02 Å, and the Fe−CN length is 1.88 Å. The iron atom essentially sits in the porphyrin plane. The out-of-plane displacement of the iron atom to the proximal histidine is only 0.06 Å with respect to the four pyrrole nitrogens, and the average Fe−N(pyrrole) length is 2.00 Å. These coordination features are consistent with ferric low-spin assignment of the heme iron coordinated with CN. Insertion of the artificial heme seriously affects the CN coordination geometry as well (Figure 5). The Fe−CN bond tilts from the heme normal by 15° toward the inner part of the heme distal cavity, and the Fe−C−N angle 165° becomes larger as compared with those found for the CN in other cyanomet Mbs (*17, 40*). The N atom of cyano ligand and Nϵ of His64 are consistently within hydrogen-bond distance of 2.65 Å, suggesting a significant interaction between them. Formation of a hydrogen bond between bound CN distal histidine is consistent with the kinetic study of the CN binding to Mb mutants (*41*).

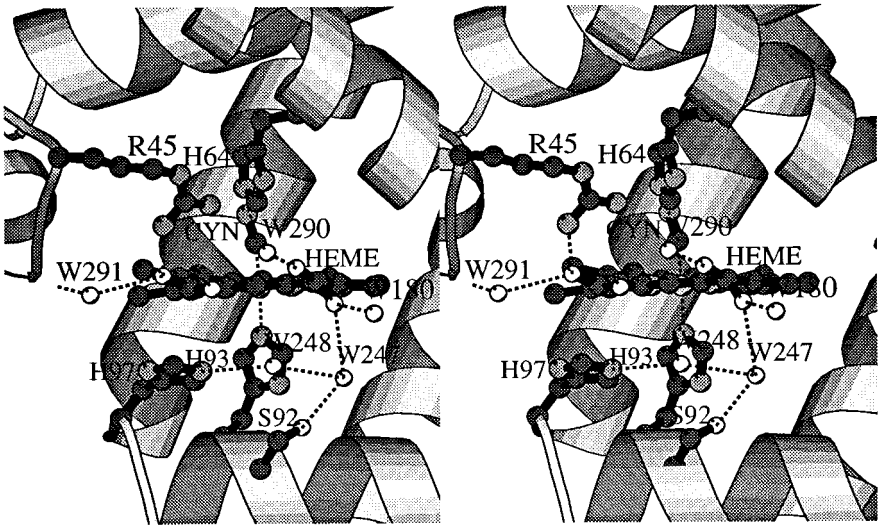

FIGURE 5: Detailed stereodrawing of the heme pocket viewed from the solvent region. Heme, iron-bound CN, the side chains of Arg45, His64, Ser92, His93, and His97, and the hydrogen-bonded water molecules are included. The broken lines denote salt bridges and hydrogen bonds.

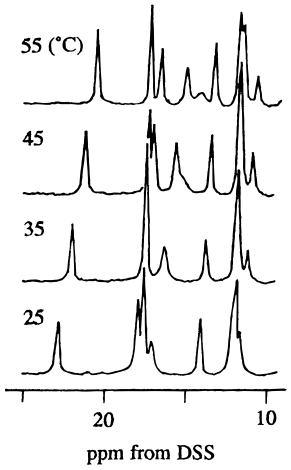

FIGURE 6: Temperature-dependent NMR spectra of the cyanomet Mb in 0.1 M Tris containing 50 mM KCN at pD 7.0. DSS = sodium 2,2-dimethyl-2-silapentane-5-sulfonate.

Temperature-Dependent NMR. A remarkable mobility difference between small hemes in crystalline and solution Mbs has been pointed out (*15*−*18*, *42*, *43*). Although the above X-ray results reveal a rigidly fixed heme in the crystalline Mb, motion of the small heme in solution Mb is not necessarily ruled out. We examined the temperature-dependent NMR to inspect heme mobility in solution Mb. The peaks observed in Figure 6 at 22.9, 18.0, 17.6, and 14.2 ppm, each with a three-proton intensity, were assigned to the heme methyls in the room-temperature spectrum. The paramagnetic shifts are linearly dependent on $1/T$ in the examined range to obey the Curie law (*35*). The NMR results are in marked contrast with those of the cyanomet Mb reconstituted with octamethylhemin (*18*), where the heme methyl signals coalesce into a single huge peak with increasing temperature due to accelerated heme rotation about the iron−histidine bond. Another notable result is thermal stability of the Mb. The concentrated Mb of about 3 mM for NMR measurement was stable to afford the well-resolved NMR spectrum up to 55 °C. Above 60 °C, the Mb thermally denatured and precipitated.

DISCUSSION

Formation of the Stable Holoprotein and Heme Electronic Modulation. The incorporation of the heme into the protein matrix is largely dependent on the hydrophobic heme−globin interactions, the covalent iron−histidine bond, and the hydrophilic interactions between the heme propionate and polar globin residues (*7*−*9*). The contributions from the heme propionates, the hydrophobic heme−globin interactions, and the iron−histidine bond to the total heme affinity are quantitatively estimated to be 25%, 50%, and 25%, respectively (*8*). The iron−histidine bond is unambiguously formed in the present Mb, and a number of specific heme−globin contacts are produced (Figure 4). These results provide structural accounts for successful incorporation of the dicarboxyhemin into the heme pocket. A high yield of the reconstitution and thermal stability of the reconstituted Mb suggest flexibility of the native apoMb to accommodate the artificial heme. The results agree with the lack of dependence of the association rates of protoheme on the exact apoMb structure as revealed from the kinetic measurements for various engineered mutants (*7*, *8*).

The specific electrostatic interactions of heme propionates are suggested to play a partial role, approximately 25% of the total, in stabilizing the heme−globin complex (*8*, *9*). Esterification of heme propionates and mutation of Arg45 produce relatively small effects on the rate of hemin dissociation. In dicarboxyheme Mb, the heme 6-propionate interaction with Arg45 is absent. Coupling of dicarboxyheme with apoMb provides additional evidence concerning the legitimacy of the original proposal (*8*). It is also notable that native globin fold is essentially conserved in dicarboxyheme Mb. Close similarity in the globin fold between the reconstituted and native Mbs is fully consistent with the previous reports that globin fold in Mb is only moderately affected by the varied heme−protein contacts (*7*−*9*, *17*, *42*−*44*).

The electron-withdrawing heme−carboxylates modulate the physical properties of the reconstituted Mb. The red-shift in visible bands of the various complexes (Table 2) is one of obvious evidence for the electronic influence of the

carboxylates through the σ bonds. The electronegative carboxylates account for the lower oxygen affinity of the reconstituted Mb as well because the oxygen affinity of Mb decreases with decreasing pK_3 of the porphyrin (*34*). It is also possible that the heme electronic states are also influenced by a single carboxylate through the π bond because the heme 6-carboxylate lies closely parallel with the porphyrin ring (Figure 5).

Unique Crystal Structure. Dicarboxyheme Mb crystallizes in the *P*6 space group. This is unique and in remarkable contrast with native Mb in $P2_1$ form (*19, 20*). Phillips (*39*) showed for the native Mb expressed in *Escherichia coli* that it is also in *P*6 form. From the comparison of the crystallographic *B*-factors between the *P*6 and $P2_1$ crystals of native Mb, he found that the heme-surrounding 40th to 60th residues are much more mobile in the former. In dicarboxyheme-bound Mb, the *B*-factors of 40th to 60th residues, 20−30 Å^2, are uniformly larger than those observed in other globin segments. The profiles of thermal fluctuation of the backbone atoms in dicarboxyheme Mb are closely similar to that of the native Mb in the *P*6 form (*39*). The difference between dicarboxyheme and protoheme was not always evident. The result suggests that increased thermal fluctuation in the CD loop and C and D helices does not directly reflect a compact dicarboxyheme structure. The *P*6 crystallization in dicarboxyheme-substituted Mb alternatively appears to relate with subtle but overall conformational changes of globin arising from the rearranged heme−globin contacts (Figures 3 and 4). Local conformational changes could change the crystal form. Several relevant examples of the *P*6 crystallization induced by a single amino acid mutation have been reported for engineered Mbs (*39, 45, 46*).

Heme−Globin Interactions. The properties of Mb are affected not only in electronic manners through the carboxylates but also in steric routes through the peripheral substituents. One notable result is a unique coordination mode of the CN. The Fe−CN axis deviates from the heme normal by 14°, while the corresponding angles for other cyano Mbs are only 3−4° (*17, 40*). The Fe−C−N angle of 165° in the present Mb is also larger than 102−127° observed in other cyanomet Mbs (*17, 40*). The distal histidine in the present Mb locates closer to the heme normal than that of porphine-bound Mb (*17*). The conformational change allows the Nϵ atom of the imidazole ring to form a hydrogen bond with the CN and pulls the N atom of the CN to the heme normal. An upright coordination of the CN is thus achieved (Figure 5).

Accelerated autoxidation of the oxy complex provides evidence for an increased polarity of the heme distal site and the rearrangements of the hydrogen-bonding networks around the heme carboxylates. Accelerated autoxidation caused by increased solvent accessibility has also been reported for recombinant Mbs. Brantley et al. (*37*) and Springer et al. (11) have shown that replacement at distal sites by amino acids incapable of hydrogen bonding to the coordinated ligand markedly increases the rate of autoxidation. The present X-ray analysis demonstrates that the networks originally formed by the heme propionates (*19, 20*) are indeed subject to intensive disruption. It is noteworthy in Figure 5 that four water molecules W180, W247, W290, and W291 attach to the short heme 6,7-carboxylates to locate closer into the hydrophobic pocket. Accelerated autoxidation of the oxy Mb is consistent with the presence of the carboxylate-attached water molecules. Adaptation of the two water molecules, i.e., W247 and W248, to the positions identical to those of the terminal oxygen atoms of the heme 7-propionate is also notable. The observation indicates an essential role of the two oxygen atoms of the heme 7-propionate in native Mb to prevent intrusion of water molecules into the hydrophobic pocket.

The heme peripheral interactions are not only important for heme incorporation but also critical in fixing orientation of the incorporated heme (*15*). The static nature of the small dicarboxyheme even at 55 °C (Figure 6) is remarkable. Since the heme is deeply embedded in the protein cavity, it is presumed that the steric constraints from the contacting globin to the six heme-methyl groups may be serious. The cramping by globin, however, seems only moderate because octamethylhemin, an all-methyl analogue for the present heme, is known to be fairly mobile in Mb (*18*). It follows that the bulkier 6,7-carboxy groups, pointing outward and making several equatorial contacts with globin, are important to settle the heme. The heme carboxylates, however, are not simple steric obstacles. The heme 6-carboxylate forms a salt bridge with the side chain of Arg45. The salt bridge is so strong that the heme is not allowed to fluctuate even at a high temperature, as evidenced by the NMR in Figure 6. Thus, the fixation of the dicarboxyheme about the iron−histidine bond predominantly arises from the single salt bridge between the heme 6-carboxylate and Arg45. The formation of this salt bridge solely depends on the remarkable conformational flexibility of the guanidinium side chain.

The implications of the present results are 2-fold. First, the reasonable structural rationale for the heme incorporation, after the extensive rearrangement of the original hydrogen-bonding networks of the heme propionates, is established. Loss of the original globin−propionate interactions is compensated with construction of the novel networks of the globin−carboxylate interactions. The reorganized hydrogen bonds and salt bridges are sufficient enough to capture the synthetic heme. The conformational flexibility of the guanidinium group in Arg45 is of particularly importance to fix the incorporated heme about the iron−histidine bond. The result invokes the previously unrecognized role of Arg45 to adopt the artificial prosthetic group with the shortest acid side chains.

Second, stable binding of the heme with the carboxylates infers the possibility of incorporation of other porphyrinoids into Mb. Various novel porphyrin isomers such as porphycene, hemiporphycene, and corrphycene with modified tetrapyrrole arrays have recently been synthesized (*47*). It is now likely that the novel porphyrinoids, after attachment of the peripheral carboxylates, can be incorporated into apoMb. The present results provide guidance and stimulus for future efforts to explore the biological aspects of these porphyrin-like macrocycles.

ACKNOWLEDGMENT

We thank Hiromi Yodo for technical assistance.

REFERENCES

1. DiNello, R. K., and Chang, C. K. (1978) in *The Porphyrins* (Dolphin, D., Ed.) Vol. 1, pp 289−339, Academic Press, New York.

2. Chang, C. K., Ward, B., and Ebina, S. (1984) *Archiv. Biochem. Biophys. 213*, 366−371.
3. Sugita, Y. (1975) *J. Biol. Chem. 250*, 1251−1256.
4. Asakura, T. (1978) *Methods Enzymol. 52*, 447−455.
5. Caughey, W. S. (1973) in *Inorganic Biochemistry* (Eichhorn, G. L., Ed.) Vol. 2, pp 797−831, Elsevier, Amsterdam.
6. Morkis, D., Brüschweiler, R., and Wright, P. E. (1993) *J. Am. Chem. Soc. 115*, 6238−6246.
7. Hargrove, M. S., Barrick, D., and Olson, J. S. (1996) *Biochemistry 35*, 11293−11299.
8. Hargrove, M. S., Wilkinson, A. J., and Olson, J. S. (1996) *Biochemistry 35*, 11300−11309.
9. Hunter, C. L., Lloyd, E., Eltis, L. D., Rafferty, S. P., Lee, H., Smith, M., and Mauk, G. (1997) *Biochemistry 36*, 1010−1017.
10. Coletta, M., Boffi, A., Ascenzi., P., Brunori, M., and Chiancone, E. (1990*) J. Biol. Chem. 265*, 4828−4230.
11. Springer, A. P., Sliger, G. S., Olson, J. S., and Phillips, G. N., Jr. (1994) *Chem. Rev. 94*, 699−714.
12. Hauksson, J. B., La Mar, G. N., Pandey, R. K., Rezzano, I, and Smith, K. M. (1990) *J. Am. Chem. Soc. 112*, 6198−6205.
13. Hauksson, J. B., La Mar, G. N., Pande, U. P., Pandey, R. K., Parish, D. W., Singh, J. P., and Smith, K. M. (1990) *Biochim. Biophys. Acta 1041*, 186−194.
14. La Mar, G. N., Hauksson, J. B., Dugard, L. B., Liddel, P. A., Venkataramana, N., and Smith, K. M. (1991) *J. Am. Chem. Soc. 113*, 1544−1550.
15. Neya, S., and Funasaki, N. (1987) *J. Biol. Chem. 262*, 6725−6728.
16. Neya, S., and Funasaki, N. (1988) *Biochim. Biophys. Acta 952*, 150−157.
17. Neya, S., Funasaki, N., Sato, T., Igarashi, N., and Tanaka, N. (1993) *J. Biol. Chem. 268*, 8935−8942.
18. Neya, S., Funasaki, N., Shiro, Y., Iizuka, T., and Imai, K. (1994) *Biochim. Biophys. Acta 1280*, 31−37.
19. Takano, T. (1977) *J. Mol. Biol. 110*, 537−568.
20. Yang, F., and Phillips, G. N., Jr. (1996) *J. Mol. Biol. 256*, 762−774.
21. Fischer, H., and Halbig, P. (1926) *Justus Liebigs Ann. Chem. 447*, 123−139.
22. Johnson, A. W., Kay, I. T., Markham, E., Price, R., and Shaw, K. B. (1959) *J. Chem. Soc*., 3416−3424.
23. Hambright, P. (1975) in *Porphyrins and Metalloporphyrins* (Smith, K. M., Ed.), pp 233−278, Elsevier, Amsterdam.
24. Adler, D., Longo, F., Kampas, F., and Kim, J. (1970) *J. Inorg. Nucl. Chem. 32*, 2443−2445.
25. Fuhrhop, J.-H., and Smith, K. M. (1975) in *Porphyrins and Metalloporphyrins* (Smith, K. M., Ed.), p 837, Elsevier, Amsterdam.
26. Teale, F. W. J. (1959) *Biochim. Biophys. Acta 35*, 543.
27. Antonini, E, and Brunori, M. (1971) *Hemoglobin and Myoglobin in Their Reactions with Ligands*, pp 10−11, North-Holland Publishing Co., Amsterdam, The Netherlands.
28. Sato, M., Yamamoto, M., Imada, K., Katsube, Y., Tanaka, N., and Higashi, T. (1992) *J. Appl. Crystallogr. 25*, 348−357.
29. Higashi, T. (1990) *J. Appl. Crystallogr. 23*, 253−257.
30. Brünger, A. T. (1992) *XPLOR 3.1 Manual*, Yale University Press, New Haven, CT.
31. Jones, T. A. (1985) *Methods Enzymol. 115*, 157−171.
32. Imai, K. (1981) *Methods Enzymol. 76*, 438−449.
33. Hayashi, A., Suzuki, T., and Shin, M. (1973) *Biochim. Biophys. Acta 310*, 309−316.
34. Sono, M., and Asakura, T. (1975) *J. Biol. Chem. 250*, 5227−5232.
35. Goff, H. M. (1983) in *Iron Porphyrins* (Lever, A. B. P., and Gray, H. B., Eds.) Part I, pp 237−281, Addison-Wesley, London.
36. Rothgeb, T. M., and Gurd, F. R. N. (1978) *Methods Enzymol. 52*, 473−486.
37. Brantley, R. E., Jr., Smerdon, S. J., Wilkinson, A. J., Singleton, E. W., and Olson, J. S. (1993) *J. Biol. Chem. 268*, 6995−7010.
38. Luzzati, V. (1952) *Acta Crystallogr. 5*, 802−810.
39. Phillips, G. N., Jr. (1990) *Biophys. J. 57*, 381−383.
40. Conti, E., Moser, C., Rizzi, M., Mattive, A., Lionetti, Coda, A., Ascenzi, P., Brunori, M., and Bolognesi, M. (1993) *J. Mol. Biol. 233*, 498−508.
41. Dou, Y., Olson, J. S., Wilkinson, A. J., and Ikeda-Saito, M. (1996) *Biochemistry 35*, 7107−7113.
42. Sato, T., Tanaka, N., Moriyama, H., Matsumoto, O., Takenaka, A., Neya, S., and Funasaki, N. (1992) *Bull. Chem. Soc. Jpn. 65*, 739−745.
43. Hata, T., Hata, Y., Sato, T., Tanaka, N., Neya, S., Funasaki, N., and Katsube, Y. (1991) *Bull. Chem. Soc. Jpn. 64*, 821−828.
44. Wagner, U. G., Müller, N., Schmitzberger W., Falk, H., and Kratky, C. (1995) *J. Mol. Biol. 247*, 326−337.
45. Quillin, M. L., Arduini, R. M., Olson, J. S., and Phillips, G. N., Jr. (1993) *J. Mol. Biol. 234*, 155.
46. Quillin, M. L., Li, T., Olson, J. S., Phillips, G. N., Jr., Dou, Y., Ikeda-Saito, M., Regan, R., Carlson, M., Gibson, Q. H., Li, H., and Elber, R. (1995) *J. Mol. Biol. 245*, 416−436.
47. Vogel, E. (1996) *J. Heterocycl. Chem. 33*, 1461−1487.

BI972632C